EFFECT OF SEVERE CORROSION ON CYCLIC DUCTILITY OF STEEL

By Michel Bruneau,[1] Member, ASCE, and Seyed Mehdi Zahrai[2]

ABSTRACT: Although some past experimental studies indicate that the monotonic structural ductility of steel is not detrimentally affected by severe corrosion, no study has investigated whether such severely rusted members can reliably exhibit the stable cyclic ductile behavior necessary for seismic survival. To generate preliminary data, a few rusted pieces taken from an existing steel bridge have been subjected to numerous cycles of alternating plasticity in flexure. Specimens had up to a 60% loss of cross-sectional area because of corrosion. This limited test program revealed that, although stable hysteretic behavior comparable with that of unrusted specimen is possible, premature failure under alternating plasticity can typically develop (in spite of satisfactory ductile behavior under monotonic loading). Irregularities along the severely rusted surface apparently act as crack initiators and precipitate crack propagation throughout the section.

INTRODUCTION

Recent earthquakes worldwide have demonstrated the potential seismic vulnerability of some types of steel bridges. Subsequently to these earthquakes, numerous transportation agencies have started programs to evaluate the seismic vulnerability of their existing bridge inventory. However, in numerous parts of North America, the seismic evaluation problem can be complicated by the fact that steel bridges have suffered years of exposition to aggressive corrosion environments, particularly where road deicing salts have been heavily used. As a result, many of the key structural members located along the critical seismic-resistance load paths of those bridges are severely corroded.

Although there is no published information on the seismic performance of severely corroded members, practicing engineers have apparently not questioned whether rusted members can still exhibit the cyclic ductile behavior and hysteretic energy-dissipation capacity commonly relied on for seismic resistance.

Some evidence seems to justify this position. First, on a material level (i.e., beyond effects resulting from the changes in cross-sectional area), metallurgical engineers involved in corrosion-related research indicate that the mechanical properties of structural steel would not be affected by corrosion damage unless (1) the microstructure of the steel of interest is modified by the corrosion process; or (2) hydrogen embrittlement is introduced as a result of the electrochemical corrosion reactions. In that regard, there is no reasonable ground to believe that the crystalline structure of steel would change significantly during ordinary atmospheric corrosion, and the possibility of hydrogen embrittlement under these conditions is also considered to be very remote, except in some applications of pickling (an electrochemical process used to remove corrosion products from metal surface), electroplating, or cathodic protection, with the risk of embrittlement increasing as the strength of the steel increases (Prof. M. Tullmin, personal communication, 1995).

Second, experimental studies on the behavior of corroded members, although few, indicate that the monotonic structural ductility of steel is not detrimentally affected by corrosion. For example, Fisher et al. (1991) conducted ultimate strength tests on two severely corroded bridge hangers having approximately 40% area loss and taken from an actual bridge. They found that the hangers could resist maximum axial loads corresponding to the tensile strength calculated using the effective net area of the most rusted region of the member, while exhibiting no considerable reduction in the monotonic structural ductility of the specimens.

In that perspective, analytical structural engineering evaluation techniques reported in the literature mostly consider the impact of corrosion due to loss of material and consequent reduction of section properties [e.g., Kayser and Nowak (1989); and Kulicki et al. (1991)]. It is recognized that the presence of severe corrosion can typically result in increased stress levels for a given load or in larger stress ranges under cyclic loading, as well as some notable shifts in the type of ultimate failure expected as some geometric properties and failure modes are related to the square or cube of member dimensions (Kayser et al. 1987; Kayser and Nowak 1989).

In the foregoing studies, procedures, and perceptions, the impact of severe corrosion on the cyclic ductile behavior and hysteretic energy dissipation of steel members, although not directly addressed, is inferred to be of no worse consequences than observed for monotonic static loadings. However, there exists some compelling reasons to undertake an experimental verification of this claim.

First, at a conceptual level, one may envision that the surface of a severely corroded structural member may have sharp irregularities that can act as crack initiators and precipitate crack propagation and failure. This has never been investigated in the seismic perspective of cyclic ductility and hysteretic energy, but this concern has received some attention by researchers concerned with high-cycle fatigue resistance. Although past studies have shown that this is not a major concern in most cases, notably, with weathering steel, for example, it remains that a limited number of fatigue-related experiments on severely corroded members (Kulicki et al. 1990; Fisher et al. 1990, 1991) indicate that, as a result of stress concentrations introduced by rust and rust-related notches, corroded base metal and details in steel bridge components could have a lower fatigue life than unrusted steel of an equivalent remaining cross-sectional area. This reduction can be important, with reported fatigue performance as low as the American Association of Highway and Transportation Officials' (AASHTO 1983) fatigue category E in the combined presence of severe corrosion notches and thickness losses in excess of 50%. For pitting corrosion, Albrecht and Simon (1981) proposed a relationship to relate pit depth to a fatigue notch factor and an equivalent corresponding fatigue category detail. However, the extent of this potential detrimental effect of severe corrosion on fatigue life is apparently difficult to quantify and a contro-

[1]Assoc. Prof., Ottawa-Carleton Earthquake Engrg. Res. Ctr., Dept. of Civ. Engrg., Univ. of Ottawa, 161 Louis Pasteur, Ottawa, Ontario, Canada, K1N 6N5.

[2]PhD Candidate, Ottawa-Carleton Earthquake Engrg. Res. Ctr., Dept. of Civ. Engrg., Univ. of Ottawa, 161 Louis Pasteur, Ottawa, Ontario, Canada.

Note. Associate Editor: Prof. Chia-Ming Uang. Discussion open until April 1, 1998. To extend the closing date one month, a written request must be filed with the ASCE Manager of Journals. The manuscript for this paper was submitted for review and possible publication on May 29, 1997. This paper is part of the ***Journal of Structural Engineering***, Vol. 123, No. 11, November, 1997. ©ASCE, ISSN 0733-9445/97/0011-1478–1486/$4.00 + $.50 per page. Paper No. 13282.

versial topic (Kulicki et al. 1990). Also, although being a related topic, it remains that research findings on the high-cycle fatigue issue cannot be extrapolated directly to the seismic problem.

Second, research is underway to seismically retrofit steel bridges using steel-based passive energy–dissipation systems (Bruneau and Zahrai 1997; Zahrai and Bruneau 1997). Some of these systems include special devices that can be subjected to very large local ductilities during earthquakes. Questions arise as to whether they can perform as intended even if rusted by the time a major earthquake strikes (in a distant future) and whether rust would affect their ability to survive repeated earthquakes (i.e., must they be replaced following a major earthquake).

Finally, on a pragmatic level, given the absence of experimental data on the impact of severe corrosion on the hysteretic energy–dissipation capacity of steel and the potential impact this may have on the seismic resistance of steel structures, a limited testing effort would be sufficient to expediently provide, if only in a preliminary way, an answer to the problem at hand.

This paper reports the findings from one such experimental research of limited scope, to establish whether the hysteretic energy–dissipation capacity of severely corroded steel is truly comparable with that of noncorroded members. For that purpose, a small number of specimens having up to a 60% loss of cross-sectional area due to corrosion were taken from a rusted existing steel bridge recently decommissioned and tested. Results from noncyclic monotonic tests are first reported, to demonstrate that the corroded steel tested is indeed found to be fully ductile when tested using traditional monotonic tension tests. This is followed by results from flexural bending tests on two different types of specimens, to various levels of ductility intensities. Contrary to what some engineers have alleged and expected (as explained in the foregoing paragraphs and heard through various personal communications) and in spite of satisfactory ductile behavior under monotonic loading, it is found that severely corroded steel exhibits a reduced resistance to alternating plasticity (also known as low-cycle fatigue). Results are presented in terms of strength, ductility, cyclic ductility, and cumulative hysteretic energy, in the perspective of seismic resistance.

Note that other serious structural effects of corrosion on structural behavior, such as freezing of bearings (that can translate into large forces in piers, abutments, and other members), freezing of pinned joints (that may create unintended bending moments in members), and the buildup of corrosion products [causing local forces and distortions transverse to the normal load–carrying direction and that have led to failures in some major bridges (Kulicki et al. 1990)], among many other detrimental effects caused by nonuniform patterns of corrosion on bridge members, are beyond the scope of this study. However, the engineer should keep those items in mind when evaluating the seismic (or general) structural performance of an existing steel bridge. Also note that, in spite of the emphasis on bridges here, the findings reported here are broadly applicable to similarly corroded members located in any type of structure if subjected to the same load and deformation conditions.

NONCYCLIC MATERIAL DUCTILITY

Even though the available literature reported in the foregoing section suggests that a ductile noncyclic behavior is somewhat anticipated, the material under consideration here was first tested under monotonically increasing static load to establish its noncyclic ductility, for better comparison with the cyclic test results presented in a subsequent section. The rusted steel specimens available for this study were obtained from a bridge constructed in Ontario in the 1950s (demolished and replaced in 1991). The original structural drawings called for medium steel, likely a CAN/CSA G40.4 structural steel (equivalent to ASTM-A7 steel) as this was the prevalent mild structural steel for buildings and bridges in those days (Kulak et al. 1995). Incidentally, all specimens taken from that decommissioned bridge exhibited uniform corrosion [this most common form of corrosion, with metal oxidation taking place somewhat uniformly over the entire exposed surface accounts for the greatest destruction of metal on a tonnage basis—see Kulicki et al. (1990)].

To obtain the complete stress-strain relationship for the existing rusted steel material, coupons were extracted from a severely rusted floor beam; two were taken from the web and one from the flange and all three were flame-cut in the longitudinal direction of the floor beam. Then, they were machined in accordance with the ASTM E8M specification [American Society for Testing and Materials (ASTM) (1995)] with a 200-mm gauge length (Davis et al. 1982) with the important exception that the wide sides of the steel coupons (corresponding to the outside surfaces of the flange and web) were left unmachined to preserve their rusted surfaces. Each coupon was marked in 25-mm intervals along its gauge length and mapped to have the coupon thickness measured at three points across at each interval, as shown in Fig. 1. Thicknesses for the entire gauge length of the three coupons, measured using a micrometer, are presented in Table 1. Maximum loss of cross-sectional area caused by corrosion, as given by the least average thickness measured across an interval, is 61.5, 36.2, and 6.3% for the flange [original thickness of 18.5 mm, as per American Institute of Steel Construction (AISC) (1953)], web 1, and web 2 (original thickness of 11.6 mm) coupon specimens, respectively.

Test results are presented in Figs. 2 and 3 in terms of strength versus elongation and stress versus strain, respectively. Stresses in Fig. 3 were obtained by dividing the applied load by the cross-sectional area at the minimum average thickness along the gauge length. Expected results for comparable unrusted specimens also are plotted in these figures, using the minimum yield strength F_y of 230 MPa (33 ksi), tensile strength F_u of 420 MPa (60 ksi), and elongation in 200 mm of 21% specified for that G40.4 steel [Canadian Institute of Steel Construction (CISC) (1962)]. Fig. 2 clearly illustrates that the expected loss of strength is directly proportional to the loss in cross-sectional area (note that flange and web coupons had different original thicknesses). All coupons failed at their section of least-measured cross-sectional area.

As shown in Fig. 3, although the yield stress threshold is not affected by the presence of corrosion, a well-defined yield plateau does not exist for the severely corroded specimens. This is logical because the cross-sectional area varies continuously along the length of the specimen due to randomness in the corrosion attack. Also shown in that figure, maximum elongations at failure ε_{max} of 14.2, 15, and 16% were obtained for the rusted coupons. This is somewhat less than the specified elongation for G40.4 (A7) steel, but this loss of ductility mostly can be attributed to slightly premature necking initiation and a shorter descending branch of the stress-strain curve

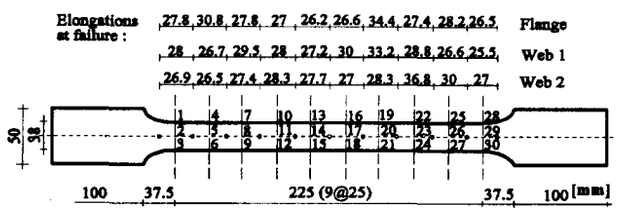

FIG. 1. ASTM E8M Rusted Coupon Specimens

TABLE 1. Thicknesses along the Gauge Length for Rusted Coupon Specimens

Location (1)	Flange Coupon Thickness (mm) (2)	Flange Coupon t_{ave} (mm) (3)	Web 1 Coupon Thickness (mm) (4)	Web 1 Coupon t_{ave} (mm) (5)	Web 2 Coupon Thickness (mm) (6)	Web 2 Coupon t_{ave} (mm) (7)
1	7.87		9.53		11.3	
2	7.49	7.47	8.64	8.07	11.58	11.35
3	7.04		6.05		11.18	
4	8.18		9.65		11.18	
5	7.32	7.18	8.46	8.37	11.38	11.2
6	6.05		7.01		11.05	
7	9.65		8.89		11.05	
8	7.92	7.93	8	8.13	10.92	11.05
9	6.22		7.49		10.18	
10	7.42		8.38		11.13	
11	8.26	7.77	7.37	7.58	11.18	11.12
12	7.62		6.99		11.05	
13	8.89		9.02		11.1	
14	8.69	8.82	7.92	8.19	11.15	11.18
15	8.89		7.62		11.3	
16	8.13		8.38		11.51	
17	8.76	8.45	7.67	7.65	11.35	11.48
18	8.46		6.91		11.58	
19	8.05		8.33		11.18	
20	6.91	7.1[a]	7.26	7.37[a]	11.23	11.16
21	6.35[b]		6.53[b]		11.07	
22	7.92		9.07		10.6[b]	
23	7.87	7.48	8.2	8.13	10.8	10.8[a]
24	6.65		7.11		11	
25	8.56		10.41		10.69	
26	7.52	7.31	8.81	8.88	11.43	11.01
27	5.84		7.42		10.92	
28	8.26		10.54		11	
29	6.81	7.22	9.53	9.72	10.8	10.87
30	6.6		9.09		10.8	

[a]Minimum average thickness.
[b]Minimum thickness at the critical section.

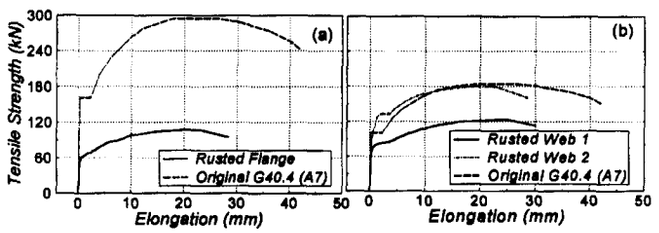

FIG. 2. Experimentally Obtained Tensile Strength of Rusted Coupons Compared with Typical Strength of Unrusted A7 Steel: (a) Flange Coupon; (b) Web Coupons

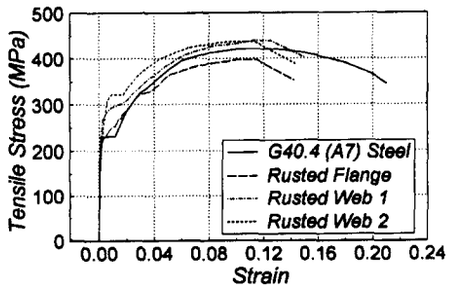

FIG. 3. Experimentally Obtained Stress-Strain Relationship for Rusted Coupons Compared with Typical Stress-Strain Curve for Unrusted A7 Steel

past that point. Considering that maximum strengths have been reached nearly at the same strain, based on this limited study of three samples, the available noncyclic material ductility can be deemed not significantly affected by the presence of corrosion, within the range of practical interest, even though it

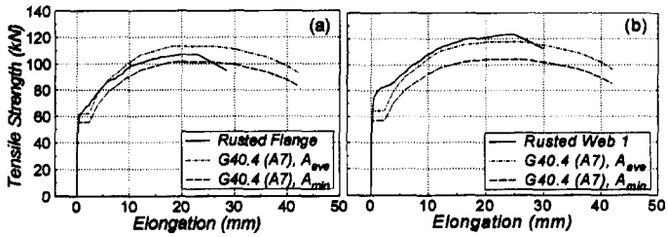

FIG. 4. Experimentally Obtained Tensile Strength of Rusted Coupons Compared with Their Theoretical Strength Normalized Using Average and Minimum Thicknesses at Critical Cross Section: (a) Flange Coupon; (b) Web 1 Coupon

was less than the minimum specified value of 21%. Finally, although the obtained ultimate stress capacity of the flange coupon is below that of the web coupons and that of the specified strength for G40.4 (A7) steel, the difference remains within statistical expectations, particularly when recognizing that the mean yield stress across the flanges of rolled shapes is usually lower than the corresponding value in their web (Galambos and Ravindra 1978). Also, it must be recognized that the true local minimum thickness could have been missed or simply been beyond reach because of the finite size of the micrometer's head.

Theoretical strength-elongation curves for the flange and web 1 coupons have been derived considering both their respective average thickness and their minimum thickness at the location along the gauge length having the smallest cross-sectional area (absolute minimum thicknesses for the specimens, located outside of the critical section where failure occurred as shown in Table 1, were not considered). These are plotted in Fig. 4 for comparison with the experimentally obtained results. As can be observed in that figure, using the least average thickness [i.e., the least remaining area as proposed by Kulicki et al. (1990)] seems a reasonable procedure, even though results can be slightly on the unconservative side.

CYCLIC BENDING TESTS

Weak-Axis Bending of Steel Plates

Two severely rusted lacing steel plates, taken from a built-up member of the decommissioned bridge, were subjected to cyclic flexure in a 3-point bending apparatus with a span of 360 mm. Obviously, lacing plates are not subjected to bending in service. However, the objective of this study is to investigate material behavior under alternating plasticity (i.e., not structural member behavior). As such, any rusted steel piece could have been used for these tests; lacing plates were simply very convenient to use.

For each plate, originally 76 mm wide and 10.5 mm thick, thickness was measured at 15 locations around the point of maximum moment, as shown in Fig. 5, and summarized in

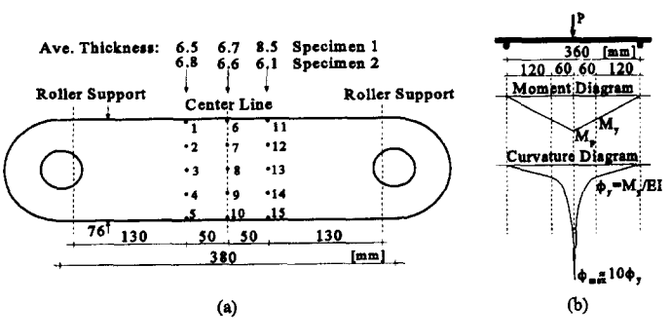

FIG. 5. Lacing Plate Specimen Subjected to Cyclic Loading: (a) Location of Measurements; (b) Loading and Corresponding Moment and Curvature Diagrams

Table 2. For the first specimen, in a first phase of testing, measurements of load versus center span deflections were taken to record the cyclic hysteretic behavior of the corroded specimens. Results are presented in Fig. 6 for the first five inelastic cycles. Onset of yielding was observed at an applied load P_y of 2.15 kN, corresponding to a midspan yield deflection δ_y of 5.8 mm, and a yield curvature ϕ_y of 0.00051 rad/mm.

Using the average measured thickness at the location of maximum moment (i.e., midspan) and steel yield strength F_y of 230 MPa, expected yield and plastic moments capacities were 0.131 and 0.196 kN·m, respectively, corresponding to applied midspan loads of 1.46 and 2.18 kN. As minimum average thickness and remaining area are synonymous, this assessment of yield strength follows the procedure recommended by Kulicki et al. (1990). Likewise, midspan deflection at first yield and the corresponding yield curvature were expected to be 3.7 mm and 0.00034 rad/mm, respectively. An expected midspan deflection of 14.8 mm at the onset of strain hardening also was estimated using the theoretical moment curvature for a rectangular cross section, a parabolically increasing curvature between the yield and plastic moments, and assuming that full plastic moment is reached at the onset of strain hardening when a curvature ductility equals 10 times the yield curvature as schematically shown in Fig. 5(b).

Given the good agreement between the experimentally obtained elastic stiffness (0.37 kN/mm) and theoretical one ($48EI/L^3$ = 0.39 kN/mm), the differences observed between experimental and analytical yield strengths and deflections can be partly attributable to the difficulty in accurately identifying experimentally the yield point for a specimen having an irregular cross section, as well as to possible slightly greater than specified yield strength of the plates tested. It is noteworthy that loss of strength caused by corrosion is considerable here, with a remaining yield strength of 2.15 kN (1.46 kN theoretical) compared with that of the noncorroded lacing plate, which would have been of approximately 3.5 kN based on the original lacing plate thickness (Ketchum 1924).

Then, to investigate the stability of these hysteretic loops under severe cyclic loading, it was decided to arbitrarily subject the specimen to 50 cycles at a maximum center deflection of 60 mm. For that specimen, this corresponded to a displacement ductility of 10.3 (i.e., 60/5.8). Statistical results by Krawinkler (1996) demonstrate that stiff structural systems can undergo a large number of inelastic excursions during severe earthquakes, but corresponding cumulative hysteretic energy demands are typically less than considered here. Nonetheless, the large ductility was selected to accumulate hysteretic energy as rapidly as possible (cycling in that particular test setup required numerous manual operations). Survival to that severe test regime would have provided confidence in the cyclic ductile capacity of rusted steel members.

In each of those large ductility cycles, a hysteretic energy of 450 kN/mm per cycle (equal to a normalized hysteretic energy $E_H/P_y\delta_y$ of 36 per cycle) was dissipated until the 28th cycle when a "popping" noise was heard. Testing was stopped and the specimen was examined. Visible on the tension side of the member was a 5-mm-long crack oriented in the width direction, approximately 1 mm wide and 1 mm deep. The crack was located approximately at midwidth and 12 mm away from the center span. A normalized cumulative hysteretic energy of 870 had been dissipated at that point. Testing resumed and an immediate drop in capacity was observed. Upon further cycling, the crack propagated in both directions, traveling toward the edges of the member as strength degradation worsened. As seen in Fig. 7(a), after the 32nd cycle, strength had fallen by 75%; the crack had spread through thickness and nearly across the entire width of the specimen, and testing was stopped. Also note that, although the deflection history was measured continuously for the first five cycles (as shown in Fig. 6), only a few measurements were taken along each hysteresis loop from the sixth cycle up to failure (Fig. 7) to accelerate the testing process. Hysteretic energy values reported for the lacing plate tests are thus slightly lower than would have been obtained using Ramberg-Osgood tracing over the recorded data point.

A second nearly identical specimen was similarly tested in an attempt to reproduce the results. Immediately from the first cycle, and in each cycle, the specimen (with P_y of 1.8 kN and δ_y of 5.2 mm) was pushed to a displacement ductility of 11.5,

TABLE 2. Thicknesses along Rusted Lacing Plates

	Lacing Plate Specimen 1		Lacing Plate Specimen 2	
Location (1)	Thickness (mm) (2)	t_{ave} (mm) (3)	Thickness (mm) (4)	t_{ave} (mm) (5)
1	6.4		7.6	
2	6.0		7.2	
3	6.2	6.5	6.4	6.8
4	6.4		7.0	
5	7.5		5.9	
6	6.1		6.7	
7	5.2		6.9	
8	7.1	6.7	7.1	6.6
9	7.3		6.5	
10	7.9		5.9	
11	8.5		5.8	
12	8.5		6.2	
13	8.5	8.5	6.4	6.1
14	8.6		5.9	
15	8.2		6.2	

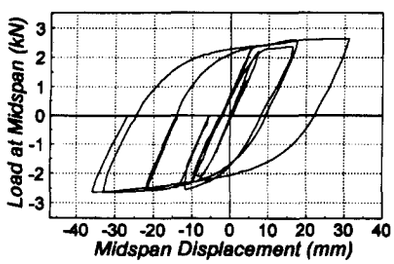

FIG. 6. Cyclic Load-Displacement Relationship for Plate Specimen 1, First Five Cycles

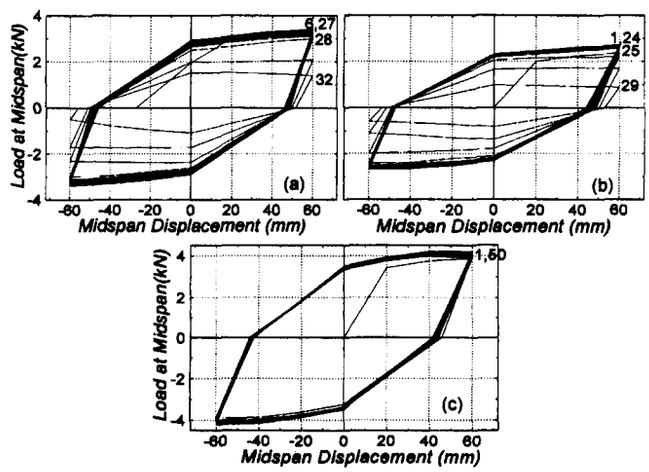

FIG. 7. Simplified Hysteretic Behavior of Plate Specimens: (a) Rusted Specimen 1, for Cycles 6 to Failure; (b) Rusted Specimen 2, All Cycles; (c) Unrusted Specimen for All Cycles

corresponding to a hysteretic energy of 362 kN/mm (normalized hysteretic energy of 39). This time, strength degradation became noticeable during the 25th cycle as shown in Fig. 7(b), after a cumulative normalized hysteretic energy of 960. Examination of the specimen's surface revealed that fine cracking had occurred across the width of the member about 10 mm from the center span. Crack propagation and strength degradation in the subsequent cycles followed the pattern previously established, thus validating previously obtained results. Final state of the specimens and cross-width cracks are shown in Fig. 8. Close-up view of the rusted specimens' surface texture in the vicinity of the crack is shown in Fig. 9. Fig 10(a) shows a typical cross-thickness view at the crack failure surface, with noticeable thickness variations, and Fig. 10(b) illustrates other cracks of finite lengths that typically developed in parallel to the failure surface.

Information on the alternating plasticity resistance (i.e., low-cycle fatigue) of structural steel indicates that at least 1,000, 100, and 20 cycles should be sustained at strains of 0.03, 0.07, and 0.15, respectively, prior to failure [American Society for Metal (ASM) (1986)]. These would approximately correspond to curvature ductilities of 25, 60, and 130, respectively. Hence, for the maximum curvature ductility of approximately 30 developed during this test, virgin steel should be able to sustain more than 800 cycles, and the preceding results thus indicate a considerable drop in low-cycle fatigue resistance. However, to confirm that the results obtained were not inadvertently influenced by the particular test setup adopted and provide an approximate experimental comparison benchmark, a new plate of mild steel (of 300-MPa yield strength) and same width as that of the rusted plates also was tested. Its thickness was chosen to be approximately equal to the least value measured on the rusted specimens (i.e., 6.3 mm). This new steel plate was subjected to 50 inelastic cycles at a center displacement of 60 mm, corresponding to a displacement ductility of 9, curvature ductility of 20, and cumulative hysteretic energy of 26,800 kN/mm for 50 cycles (normalized cumulative hysteretic energy of 1,640) without any sign of cracking or strength reduction. Results are shown in Fig. 7(c) for comparison.

Conceptually, the aforementioned observed premature cracking under alternating plasticity can be attributed to the presence of irregularities along the rusted surface that act as crack initiators and precipitate crack propagation throughout the section. Consequently, members with large corrosion notches or more severe levels and types of corrosion than considered here would likely have an even lower cracking resistance under alternating plasticity.

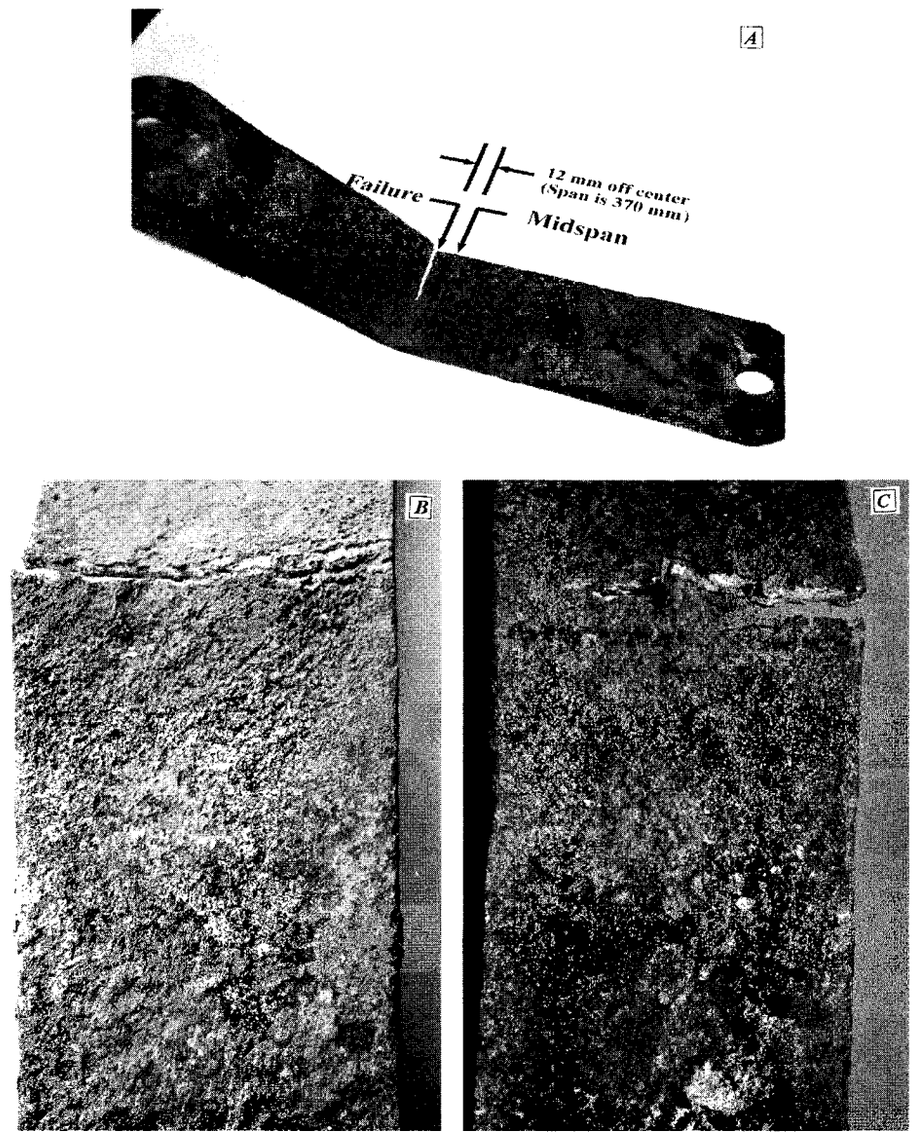

FIG. 8. Final State of Plate Specimens and Cross-Width Cracks: (a) Global View of Specimen 1 after Test; (b) Cross-Width Cracking for Specimen 1; (c) Cross-Width Cracking for Specimen 2

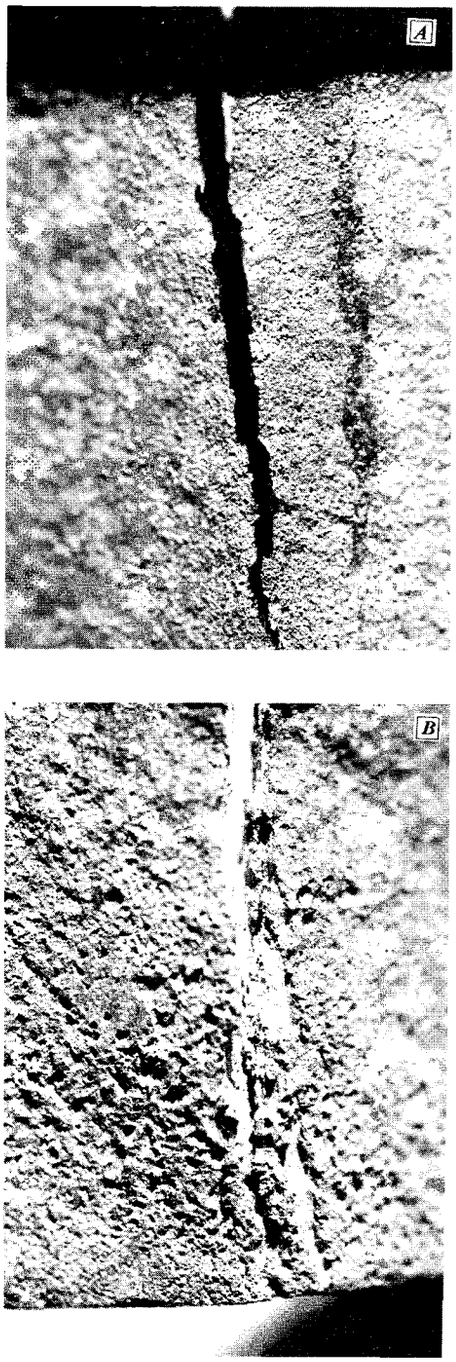

FIG. 9. Close-Up View of Surface Texture for Three-Point Bending Specimens: (a) First Cracking Side for Specimen 1; (b) Last Ruptured Side for Specimen 2

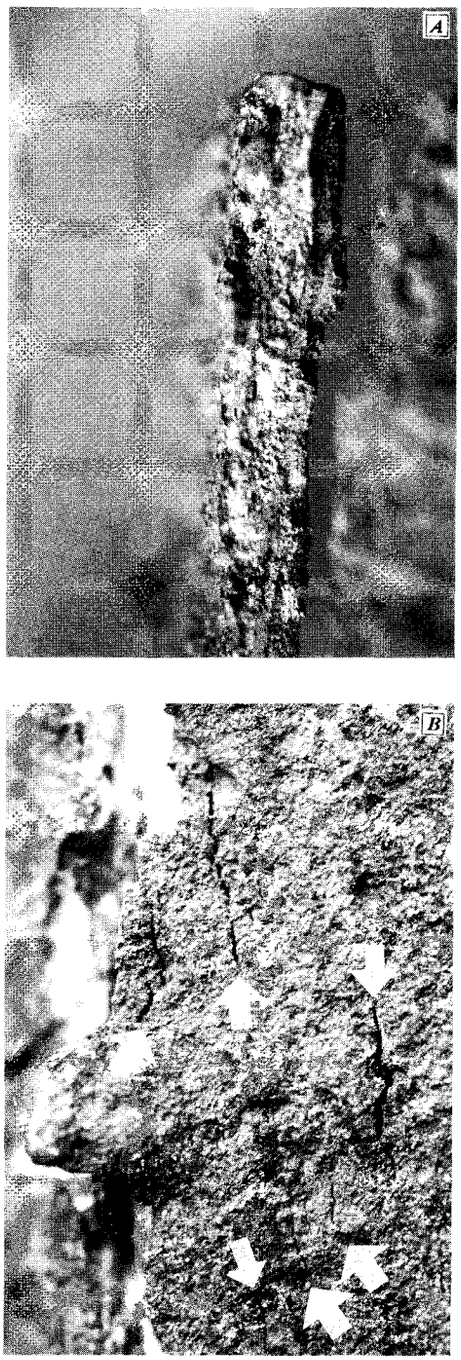

FIG. 10. Close-Up View of: (a) Typical Failure Surface of Irregular Thickness; (b) Other Cracks of Finite Lengths Parallel to Failure Surface

Out-of-Plane Bending of Web of Structural S-Shape

Although the foregoing information provided evidence that corrosion has a detrimental effect on the alternating plasticity resistance of structural steel, at least for the severity and type of corrosion considered, failure occurred at large displacement ductilities, after a considerable amount of hysteretic energy was dissipated. Hence, additional tests were deemed necessary to determine whether similar failures would still occur at lesser ductilities.

The severely rusted web of a 350-mm-long floor beam segment flame-cut from the same aforementioned bridge was found to be most suitable for this next phase of testing. A simple setup made it possible to subject the rusted web plate of this structural member to cyclic out-of-plane flexure without the need to extract any material or otherwise disturb the rusted region. As shown in Fig. 11, the flange of the structural shape was bolted down to a rigid steel base itself anchored to a strong reaction floor. Bolts were placed as close as possible to the web of the specimen to effectively eliminate its rotation due to flexure of the flange. A horizontally placed servocontrolled actuator connected at midheight of the web was used to cycle the cantilevering web in flexure about its weak axis, henceforth testing the most severely rusted portion of the web, which happened to be near the web-flange intersection. Moreover, by simply flipping the specimen upside down, it was also possible to test the second most rusted part of the web, located near the other web-flange intersection. Again, this was done as a convenient way to perform alternating plasticity tests on

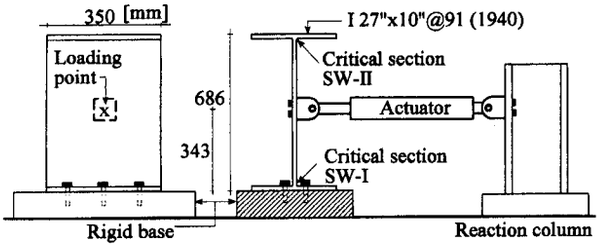

FIG. 11. Test Setup for Weak-Axis Bending of Floor Beam's Rusted Web

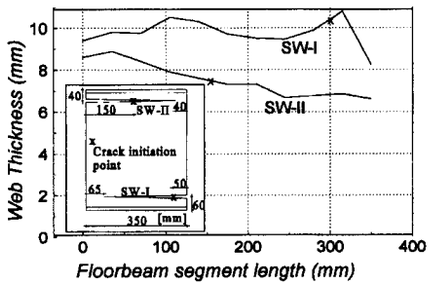

FIG. 12. Web Thickness in Critical Areas where Cracking Happened for Two Specimens

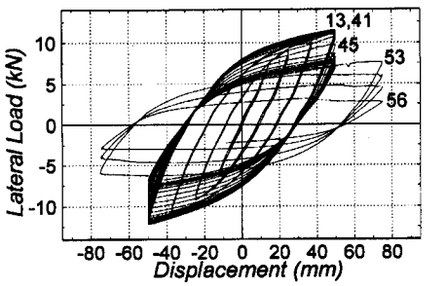

FIG. 13. Hysteretic Load–Displacement Curves for Floor Beam Web Specimen 1 (SW-I)

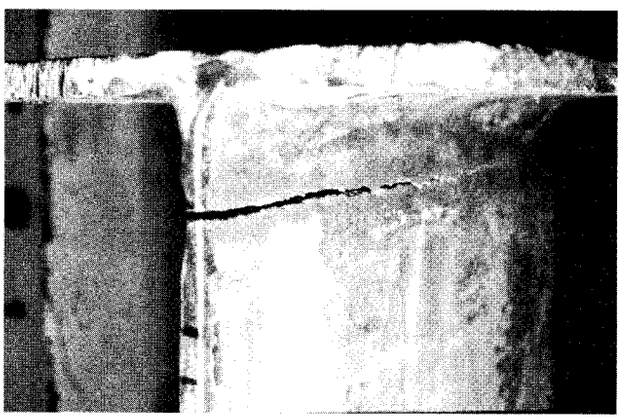

FIG. 14. Specimen SW-I after Testing (Upside Down) Showing Final Crack Length and Opening

rusted material and is obviously not intended to replicate actual seismic effects on a floor beam.

Preparation of the specimen was limited to extensive grinding of the ends of the floor beam segment to smoothen the flame-cut surfaces and eliminate the possible presence of a martensite layer there, as well as any jagged edge, notch, or any other stress raiser that could trigger crack initiation unrelated to the presence of corrosion. Prior to testing, thickness of the web in the critical areas (i.e., near the flanges) was measured with a micrometer, as shown in Fig. 12, and was found to vary between 6.7 and 12 mm, with average thick-

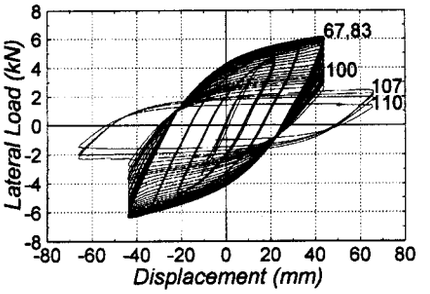

FIG. 15. Hysteretic Load–Displacement Curves for Floor Beam Web Specimen 2 (SW-II)

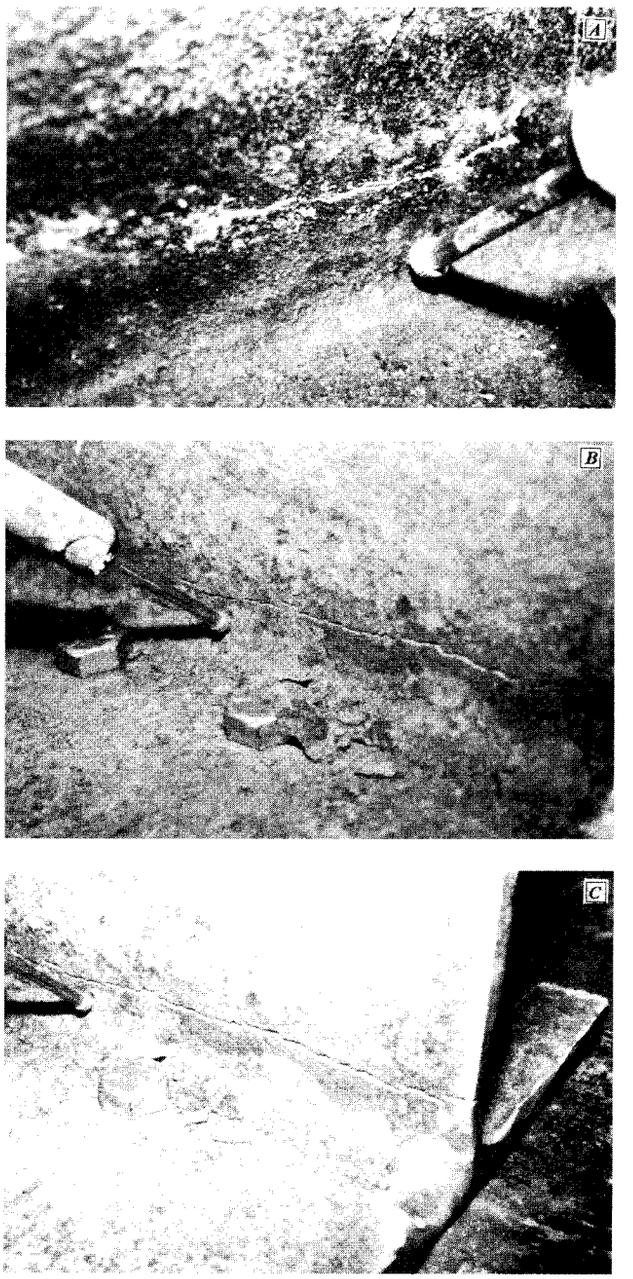

FIG. 16. Progression of Cracking in Specimen SW-II: (a) Early Cracking on East Face; (b) Same on West Face; (c) Significant Crack Propagation on West Face

nesses of 9.8 and 7.5 mm at the critical section of specimens SW-I and SW-II, respectively, i.e., the first and second tests of this sequence. Original unrusted web thickness was 12.3 mm (AISC 1953).

TABLE 3. Displacement Ductility and Hysteretic Energy Values for SW-I and SW-II Specimens

S-SHAPE WEB 1 (SW-I) TEST						S-SHAPE WEB 2 (SW-II) TEST					
	Displacement		Load	E_H	ΣE_H		Displacement		Load	E_H	ΣE_H
Cycle (1)	mm (2)	δ_y (3)	(kN) (4)	(kN/mm) (5)	(kN/mm) (6)	Cycle (7)	mm (8)	δ_y (9)	(kN) (10)	(kN/mm) (11)	(kN/mm) (12)
1–3	6.3	0.5	3.0	0	0	1–3	5.5	0.5	2.0	0	0
4–6	12.5	1	6.2	14.7	44	4–6	11	1	3.3	11	33
7–9	25	2	9.0	243	773	7–36	22	2	4.7	109	3,300
10–12	37.5	3	10.0	823	3,242	37–66	33	3	5.5	272	11,460
13–41	50	4	11.2	1,045	33.547	67–89	44	4	6.1	479	22,477
42–43	50	4	11.0	960	35,467	90–91	44	4	5.8	435	23,347
44	50	4	10.8	914	36,381	92–94	44	4	5.5	418	24,601
45	50	4	9.8	874	37,255	95	44	4	5.0	395	24,996
46	50	4	8.4	800	38,055	96–98	44	4	4.5	366	26,094
47	50	4	8.2	725	38,780	99–100	44	4	3.9	340	26,774
48–52	50	4	7.5	663	42,095	101–103	44	4	3.6	306	27,692
53	75	5	7.7	1,170	43,265	104–105	44	4	3.1	278	28,248
54	75	5	6	1,114	44,379	106	44	4	2.7	253	28,501
55	75	5	4.6	1,028	45,407	107	55	5	2.4	397	28,898
56	75	5	2.6	857	46,264	108–109	55	5	2	376	29,650
						110	55	5	1.3	350	30,000
$\Sigma E_H/P_y\delta_y = 600$						$\Sigma E_H/P_y\delta_y = 820$					

Instrumentation was limited to a load cell and LVDT internal to the actuator and 3 other LVDTs set to monitor slippage of the specimen base and rotation at the web-flange intersection (these actually revealed that none occurred). A high-resolution data acquisition system was used to record all data during the cyclic hysteretic testing of the corroded specimen. Because analytical estimates of the yield displacement proved difficult to calculate accurately, each test started by first subjecting the specimen to a few cycles of loading in search of the yield displacement, followed by a preprogrammed hysteretic displacement history constructed using this yield value. For the first test (SW-I), yield displacement was judged to occur at 12.5 mm based on first visible evidence of hysteretic behavior on real-time plots of load-displacement curve. The hysteretic displacement history was then programmed to apply three cycles at each of the displacements of $\pm 0.5\delta_y$, $\pm 1.0\delta_y$, $\pm 2.0\delta_y$, and $\pm 3.0\delta_y$, followed by 40 cycles at $\pm 4.0\delta_y$, 20 cycles at $\pm 6.0\delta_y$, and cycling to failure at $\pm 8.0\delta_y$. This follows the spirit of the ATC-24 testing protocol [Applied Technology Council (ATC) (1992)], albeit with more cycles at the range of inelastic deformations where alternating plasticity–resistance data is sought. Loading rate was 1.0 cycle/min.

The resulting load-displacement hysteretic curves for the first test are shown in Fig. 13 (SW-I). During testing, a drop in the applied load necessary to push the specimen to displacements of $\pm 4.0\delta_y$ was noticed during the 40th load cycle (counting from the beginning of testing). This prompted closer examination of the specimen and discovery that a small hairline crack had appeared on both faces of the web, at roughly 50 mm from the south edge of the specimen and 60 mm above the base of the specimen (Fig. 12). Five cycles later, the visible horizontal crack had grown to a length of 12.7 and 11.4 mm on the east and west web faces, respectively. Strength degradation of 20% was observed after the 46th cycle (i.e., after 34 cycles at $4.0\delta_y$). By the 51st cycle, crack length had reached 26.6 and 14.5 mm on the east and west faces, respectively, and strength had dropped nearly 40%. On completion of the first cycle at $\pm 6.0\delta_y$, the crack had grown to a visible length of 270 and 184 mm on the east and west faces, tearing the specimen up to its south edge. Testing was stopped after the 56th cycle, at a ductility of $6.0\delta_y$, with only a 65-mm-length of uncracked steel at the web's north edge and an 80% strength degradation. Largest crack opening was approximately 4 mm (Fig. 14).

The specimen was then flipped and a similar procedure was followed for testing the second severely corroded web area, with the difference that a different loading history was programmed to investigate the alternating plasticity resistance of the specimen when subjected to more cycles of lower ductility demand, with three cycles at each of displacements of $\pm 0.5\delta_y$ and $\pm 1.0\delta_y$, 30 cycles at each of displacements of $\pm 2.0\delta_y$ and $\pm 3.0\delta_y$, followed by 40 cycles at $\pm 4.0\delta_y$, 20 cycles at $\pm 6.0\delta_y$, and cycling to failure at $\pm 8.0\delta_y$. For this test (SW-II), yield displacement was judged to occur at 11 mm, as per the foregoing definition. The resulting load-displacement hysteretic curves for the second test are shown in Fig. 15.

The specimen was very closely inspected throughout testing and a small 40-mm-long hairline crack was first observed on the east face 150 mm from the south edge of the specimen at the 83rd cycle (corresponding to the 17th cycle at $\pm 4.0\delta_y$) as shown in Fig. 12. First visible crack on the west face was only observed at the 88th cycle; it was 20 mm long and located 135 mm from the south face, at 40 mm above the base of the specimen. Cracks rapidly grew in length and width on further cycling, as shown in Fig. 16, with lengths of 65, 75, and 194 mm on the east face and 132, 140, and 165 mm on the west face at the 90th, 98th, and 102nd cycles, respectively. Strength degradation of 20% was observed after the 96th cycle (i.e., after 30 cycles at $4.0\delta_y$). Cracking reached the south edge of the specimen on both the east and the west faces simultaneously at the 105th cycle (still at a displacement of $4.0\delta_y$) and reached the north edge on the west face at the 108th cycle (at a displacement of $6.0\delta_y$ since the 107th cycle), with 40 mm left of uncracked steel on the east face. Testing was stopped after the 110th cycle, after a strength loss of 80%.

To provide further perspective on the results of these tests, displacement ductility, hysteretic energy, and cumulative hysteretic energy per cycle, as well as corresponding normalized energy values, are presented in Table 3. It is notable that the definitions of yield strength and displacement have a considerable impact on all normalized quantities presented in this study, such as ductilities and normalized energies, particularly given the difficulty in defining this yield point, both experimentally and analytically, for the type of rusted specimens under consideration. Because the 0.2% rule was found to be impracticable here, yield was defined generously as the onset of nonlinear behavior. If, in hindsight, yield point was defined by the intersection of the asymptotes to the experimentally obtained initial stiffness and stiffness at maximum resistance, to represent behavior by a bilinear model with strain hardening

as frequently done in earthquake engineering, yield displacements would typically become approximately 20 and 17 mm for SW-I and SW-II, making all calculated ductilities considerably smaller (with failures occurring at the same number of cycles, but typically at $2.5\delta_y$ rather than at $4.0\delta_y$, with considerably more alarming consequences).

CONCLUSIONS

A limited test program was cnducted to investigate the effect of severe uniform corrosion on the hysteretic energy–dissipation capacity of structural steel. Initial tests confirmed that the noncyclic ductility of the few corroded structural steel specimens considered here was not significantly affected by the presence of rust, in spite of severe area loss, when subjected to a monotonic tension loading condition. However, cyclic flexural tests on structural members revealed that, although stable hysteretic behavior comparable with that of unrusted specimens is possible, premature fracture under alternating plasticity (i.e., low-cycle fatigue) will typically develop. These fractures may be conceptually explained by the presence of irregularities along the rusted surface that may act as crack initiators and precipitate crack propagation throughout the section.

A considerable cumulative hysteretic energy can be dissipated prior to the development of fatal cracking, and it is sufficient to provide adequate seismic resistance in most applications. However, the observed reduced ductile behavior could be an issue in some specialty applications, such as with some types of passive energy dissipation devices in which steel plates can be subjected to very high local flexural ductility demands; in such cases, preliminary findings in this paper suggest that rust protection or replacement of the devices after severe earthquakes would be warranted. Furthermore, members having large corrosion notches or more severe levels and types of corrosion than considered here may be even more significantly affected and deserve further experimental study.

Findings from these explorative tests are largely qualitative, based on a small number of specimens, and obviously not in a format usable in design. Also, the reader is warned that only behavior in bending has been studied and that the effects of severe corrosion on the cyclic ductility of members subjected to other stress conditions (e.g., axial or combined axial and bending) may be different. However, this paper provides some much-needed preliminary data and hopefully some guidance for future research in that direction.

FUTURE RESEARCH NEEDS

Although results from the limited study reported here have illustrated the propensity to premature alternating plasticity failure of rusted steel, many questions remain unresolved. Much testing is still necessary to correlate quantitatively the degree and type of severe corrosion with the plastic strains and corresponding normalized hysteretic energy to failure and generate statistical data that can be used reliably by practicing engineers. Currently, one such project is underway at the University of Ottawa, where attempts will be made, in parallel, to establish correlations between the generated results, cross-sectional properties, and maps of the roughness of surface asperities as measured by various instruments and techniques.

Analytical models capable of accounting for accurate and continuous maps of thickness variations along and across structural elements also are needed to permit calculation of the full strength-deformation envelops of severely corroded members in the inelastic range (cross-sectional loss alone is a parameter of limited usefulness in that perspective).

Finally, the effect of severe corrosion on welded structures also should be investigated; recognizing the sensitivity of welds to small defects and cracks and the impact of these defects on ductility, even in new unrusted structures, it would be reasonable to expect that severe corrosion could potentially worsen the negative impact of lack-of-penetration or lack-of-fusion defects in groove welds or undercut defects in fillet welds.

ACKNOWLEDGMENTS

The writers acknowledge the Ministry of Ontario and, more specifically, Mr. Roger Dorton, Manager, Structural Office, and Mr. Wade Young, Senior Structural Engineer, Central Region, for donation of the rusted steel bridge material used in this study. Mr. Stephen Burke and Mr. Lowell Keaths, undergraduate research assistants, also provided a useful experimental contribution to parts of this project. Financial support through a Strategic Grant of the Natural Sciences and Engineering Research Council of Canada is greatly appreciated. The second writer is grateful for the Ministry of Culture and Higher Education of Iran's support through a graduate scholarship. However, the findings and recommendations in this paper are those of the writers and not necessarily those of the sponsors.

APPENDIX. REFERENCES

Albrecht, P., and Simon, S. (1981). "Fatigue notch factors for structural details." *J. Struct. Engrg.*, ASCE, 107(7), 1279–1296.

American Association of State Highway and Transportation Officials. (1983). *Standard specification for highway bridges.* AASHTO, Washington, D.C.

American Institute of Steel Construction. (1953). *Iron and steel beams 1873 to 1952.* AISC, Chicago, Ill.

American Society for Metal. (1986). *Atlas of fatigue curves*, H. E. Boyer, ed., ASM, Materials Park, Ohio.

American Society for Testing and Materials. (1995). *Annual book of ASTM standards.* ASTM, Philadelphia, Pa.

Applied Technology Council. (1992). *Guidelines for cyclic seismic testing of components of steel structures.* Publication ATC-24, Palo Alto, Calif.

Bruneau, M., and Zahrai, S. M. (1997). "Ductile end-diaphragms to seismically protect substructures of slab-on-girder steel bridges." *5th Int. Colloquium on Stability and Ductility of Steel Struct.*, Nagoya, Japan.

Canadian Institute of Steel Construction. (1962). *Structural steel material specifications.* CISC, Toronto, Ontario, Canada.

Davis, H. E., Troxell, G. E., and Hauck, G. F. W. (1982). *The testing of engineering materials.* McGraw-Hill, Inc., New York, N.Y.

Fisher, J. W., Yen, B. T., and Wang, D. (1990). "Fatigue strength of riveted bridge members." *J. Struct. Engrg.*, ASCE, 116(11), 2968–2981.

Fisher, J. W., Yen, B. T., and Wang, D. (1991). "Corrosion and its influence on strength of steel bridge members." *Transp. Res. Rec. No. 1290*, Transportation Research Board, Washington, D.C., 211–219.

Galambos, T. V., and Ravindra, M. K. (1978). "Properties of steel for use in LRFD." *J. Struct. Engrg.*, ASCE, 104(9), 1459–1468.

Kayser, J. R., Malinski, T., and Nowak, A. S. (1987). "Corrosion damage models for steel girder bridges." *Proc. on Effects of Damage and Redundancy on Structural Performance*, ASCE, 9–22.

Kayser, J. R., and Nowak, A. S. (1989). "Capacity loss due to corrosion in steel-girder bridges." *J. Struct. Engrg.*, ASCE, 115(6), 1525–1537.

Ketchum, M. S. (1924). *Structural engineer's handbook.* McGraw-Hill, Inc., New York, N.Y.

Krawinkler, H. (1996). "Cyclic loading histories for seismic experimentation on structural components." *Earthquake Spectra*, 12(1), 1–12.

Kulak, G. L., Adams, P. F., and Gilmor, M. I. (1995). *Limit states design in structural steel.* 5th Ed., Canadian Institute of Steel Construction, Markham, Ontario, Canada.

Kulicki, J. M., Prucz, Z., Sorgenfrei, D. F., Mertz, D. R., and Young, W. T. (1990). "Guidelines for evaluating corrosion effects in existing steel bridges." *NCHRP Rep. No. 333*, Transp. Res. Board, Nat. Res. Council, Washington, D.C.

Zahrai, S. M., and Bruneau, M. (1997). "Capacity design principles and ductile end-diaphragms to seismically retrofit slab-on-girder steel bridges." *25th Can. Soc. for Civ. Engrg. Annu. Conf.*, Sherbrooke, Canada.